DOI:
10.1021/acs.jpcc.7b00924

Document Version
Peer reviewed version

Ethylene Dissociation on Ni_3Al (111)

Junning Li[1], Yu Wang[1], Davide Curcio[2], Silvano Lizzit[3], Alessandro Baraldi,[2,3,4], Lev Kantorovich[5*] and Andrea Floris[6*]*

[1]School of Physics and Technology, Wuhan University, Wuhan 430072, China
[2]Physics Department, University of Trieste, Via Valerio 2, 34127 Trieste, Italy
[3]Elettra-Sincrotrone Trieste S.C.p.A., Strada Statale 14 Km 163.5, 34149 Trieste, Italy
[4]IOM-CNR, Laboratorio TASC, AREA Science Park, S.S. 14 Km 163.5, 34149 Trieste, Italy
[5]Department of Physics, King's College London, London, Strand WC2R 2LS, United Kingdom
[6]School of Mathematics and Physics, University of Lincoln, Brayford Pool, LN6 7TS Lincoln, United Kingdom.

*afloris@lincoln.ac.uk; [*]lev.kantorovitch@kcl.ac.uk; *yu.wang@whu.edu.cn

CORRESPONDING AUTHORS
Andrea Floris, School of Mathematics and Physics, University of Lincoln, Brayford Pool, LN6 7TS Lincoln, United Kingdom, phone: +44 1522 83 5884.
Lev Kantorovich, Department of Physics, King's College London, London, Strand WC2R 2LS, United Kingdom, phone: +44 020 7848 2160.
Yu Wang, School of Physics and Technology, Wuhan University, Wuhan 430072, China, phone: +86 1587 135 1027.

ABSTRACT

Combining density functional theory, Nudged Elastic Band and high-energy resolution x-ray photoelectron spectroscopy experiments, we study the early stages and reaction pathways whereby ethylene molecules decompose on Ni_3Al (111) prior to graphene nucleation and growth. After characterizing stable configurations of ethylene on the surface, and of all intermediate products leading to carbon species, we calculate energy barriers for all relevant processes, including dehydrogenation, isomerization, C-C cleavage and their respective inverse reactions. This quantitative analysis helps in identifying the most probable reaction pathways. The combination of temperature dependent C 1s core level photoelectron spectroscopy measurements and of core level shift calculations for all the different species investigated allow us to understand the temperature evolution of the surface species, and to identify the whole reaction mechanism. Combined analysis of this kind is useful for understanding which species are present on the surface at various temperatures during chemical vapor deposition graphene growth experiments.

1 Introduction

Graphene is a system exhibiting impressive properties, which can be used in various technological applications, hence the methods that enable its large-scale production need to be investigated and exploited. These include, among many others, interfaces made of graphene coupled with 2D dielectrics[1,2,3,4], very important in high-performance nano-electronic applications.

Some of the most promising techniques for graphene production are based on epitaxial methods[5], such as chemical vapor deposition (CVD) techniques[6,7,8,9], including temperature-programmed growth (TPG)[6,8,10]. In CVD, hydrocarbon molecules in the gas-phase are deposited on a metallic substrate with catalytic properties, usually keeping the sample at a rather high temperature. In TPG hydrocarbon feedstock is deposited at low T, and successively heated. In both cases, at sufficiently high temperatures, a sequence of thermally induced chemical reactions leads to the formation of pure carbon species and, ultimately, to graphene.

A relevant stage of graphene formation is related to the initial sequence of steps that result in the formation of carbon-only species from the hydrocarbon feedstock on the bare metallic substrate. Many theoretical studies about the process of hydrocarbon molecules decomposition on catalytic transition metal surfaces exist in literature. Dehydrogenation reactions of methane and ethylene decomposition have been investigated on copper surfaces [11,12]. Density Functional Theory (DFT) and kinetic Monte-Carlo methods have been used to find pathways of ethylene reactions involving hydrogenation, dehydrogenation and isomerization reactions on Pt(111) and Pd(111)[13,14]. Comprehensive studies of C_nH_m species reactions on Pt(111) and Pt(211) are reported in Refs. 15,16, also including C-C cleavage[15]. A comparative DFT-based study on ethylene decomposition on M(111) surfaces (M= Pd, Pt, Rh, Ni) has been performed[17]. More recently, a combined theoretical-experimental analysis of ethylene decomposition and of the temperature evolution of the different species towards graphene on metal Ir(111) has been performed by Tetlow *et al.*[18]. In general, these studies have focused on monometallic transition metal surfaces.

On the other hand, on bimetallic substrates hydrocarbons generally exhibit different reaction paths compared to the parent transition metal surfaces. In many cases the energy barriers for the individual dissociation steps are comparatively lower, as found, for example, in acrolein (CH_2=CH-CH=O) decomposition and hydrogenation on several Pt-M(111)

arrangements (M=Ni, Co, Cu)[19,20,21], in H_2 and cyclohexene reactions on Pt/Ni(111)[22] and in other comparative studies of monometallic substrates (Ni, Pt, Pd, Mo, W, Fe) and their bimetallic alloys[23]. Besides these improved catalytic properties, the use of bimetallic substrates in graphene formation can allow the fine tuning of the graphene-substrate adhesion[24], and is important for the realization of more complex and technologically relevant systems. Omiciuolo *et al*.[25] have shown in this respect that after a graphene monolayer is formed, aluminum-based bimetallic substrates such as Ni_3Al are suitable for oxygen intercalation at the graphene/metal interface and for a selective oxidation of their top layers, allowing the realization of interfaces made of graphene and high-κ 2D dielectrics like Al_2O_3. Due to the low cost of Al-based bimetallic substrates, these interfaces can be created in a cheap and simple way, also exploiting their large availability and variety capable of breaking the C–H bonds in hydrocarbons.

However, detailed knowledge at the atomic level of the mechanisms of graphene formation on bimetallic substrates, including all possible dissociation paths of hydrocarbons on their surfaces, is largely missing.

The main objective of this work is an *ab initio* investigation, based on DFT and the Nudged Elastic Band (NEB) method, describing these mechanisms for ethylene adsorbed on $NiAl_3$(111). First, we identify the stable structures of an ethylene molecule on Ni_3Al(111) and all possible intermediate reaction products during its decomposition towards pure carbon species. Second, we calculate the energy barriers for all relevant reactions and we evaluate a series of dissociation pathways that include all possible reaction types (dehydrogenation, hydrogenation, isomerization and C-C cleavage/bonding). The combination of synchrotron-based temperature programmed x-ray photoelectron spectroscopy (TP-XPS)[26] with theoretically calculated values of the C 1s core level shifts for all the non-equivalent carbon atoms within every species has been crucial for identifying the nature of the species appearing at different temperatures during the whole decomposition process. This allowed us to determine the reaction pathway of the ethylene conversion into pure carbon products on $NiAl_3$(111).

2 Methods

Experimental Methods. The high energy resolution photoelectron spectroscopy measurements have been performed at the SuperESCA beamline of the Elettra synchrotron

radiation facility in Trieste, Italy. The experimental chamber (background pressure always better than $2x10^{-10}$ mbar) is equipped with a 150 mm mean radius SPECS hemispherical electron energy analyser. The overall experimental energy resolution for the C1s spectra was 50 meV with a photon energy of 400 eV. The Ir(111) single crystal was cleaned by Ar ion sputtering at room temperature (E=1.5 keV), annealing to 1400 K, with subsequent oxygen cycles to remove carbon (temperature ramps in oxygen pressure $P=1x10^{-7}$ mbar were performed between 570-1070 K) and a final H_2 treatment to remove residual oxygen traces (temperature ramps in hydrogen pressure $P=5x10^{-8}$ mbar were performed between 300-770 K). Surface cleanliness was checked by inspecting C 1s, S 2p and O 1s signals and by measuring the Ir $4f_{7/2}$ signal, which is known to show a surface CLS of -550 meV when the surface is clean[27]. After the cleaning procedure, low energy electron diffraction images displayed bright and narrow integer order diffraction spots with a low background. Spot profile analysis (Omicron SPA-LEED) of the diffraction spots corresponding to the (1x1) clean surface shows that the average terrace width in our crystal is 500 Å. C_2H_4 was dosed at T=80 K, and C coverage was calibrated by comparing the C 1s peak integral area to the spectra for a full graphene layer grown following the procedure in Ref. 25, which was considered to have a carbon coverage of 2 ML: coverages should be intended as carbon atoms per surface atom.

Theoretical Methods. Density functional theory (DFT) and NEB calculations were performed with the planewave-pseudopotential package Quantum ESPRESSO[28], using Ultrasoft pseudopotentials[29] with a wave function (charge) energy cutoff of 463 eV (4630 eV) and a GGA-PBE [30] exchange-correlation functional. Dispersion interaction was included through the self-consistent VV10 functional[31] in the rVV10 implementation[32]. We used a (4 × 4) unit cell. The Brillouin-zone was sampled with a grid of (3x3x1) **k**-points. A Methfessel-Paxton smearing of 0.16 eV was used. The Ni_3Al (111) substrate was constructed with the TETR package[33] and modeled using a periodically repeated slab of three layers, allowing a vacuum gap between the adsorbed molecular species and the bottom layer of the slab replica of ~20 Å. The top two layers of the slab were allowed to relax. Forces were relaxed up to 0.026 eV/Å, with a 1.36 x 10^{-7} eV cut-off for the total energy. All parameters have been chosen to make sure that the calculations are well converged.

Core level shifts are obtained from the C 1s electron binding energy (E_{CLS}) of a particular C atom within a C_nH_m species. We calculated E_{CLS} as the difference between the energy of an excited system (species adsorbed on the substrate) where the C 1s core electron is promoted

to the valence band (creating a hole in the core) and the energy of the unexcited (ground state) system:

$$E_{CLS} = E\,(n_c\text{-}1) - E(n_c)$$

where n_c is the number of C core electrons in its ground state. Our calculations are performed within the final state approximation of Ref. 34, where the hole is screened by the valence electrons; the latter relax after the 1s electron is promoted, but the core is kept frozen. The lack of core relaxation and the fact that the promoted electron is not actually removed from the system makes the absolute value of the binding energy inaccurate for the direct comparison with the experiment[34]. However, relative binding energies, *i.e*. differences with respect to a reference system (*e.g*., an adsorbed ethylene molecule), have been validated for a set of systems [34, 18] and are accurate within 20-50 meV[34]. This accuracy comes from the fact that the core relaxes in similar ways when a C atom experiences different chemical environments. The relative binding energies are denoted as core level shifts.

Note that our theoretical C 1s core level shifts include the effects of the adsorption degeneracies that happen for some of the species due to the reduced symmetry of the $Ni_3Al(111)$ substrate (as compared to the case of a pure parent metal).

3 Results and Discussion

The ethylene molecule and the $Ni_3Al(111)$ surface are presented in Fig. 1. Ni_3Al is an alloy of the A_3B type with an $L1_2$ structure, which crystallizes in the fcc lattice. In the $Ni_3Al(111)$ substrate each layer has a hexagonal structure with one Al atom at the centre of a hexagon formed by six Ni atoms that give a (2x2) structure, with Al atoms moving outwards with respect to the Ni-atom plane[35]. Taking into account also the relative position of the second and third layers, nine high symmetry non-equivalent adsorption sites are identified on the surface (see Fig.1): two top sites (on Ni and Al, denoted T1 and T2, respectively), four hollow sites (H1-H4), and three bridge sites (B1-B3).

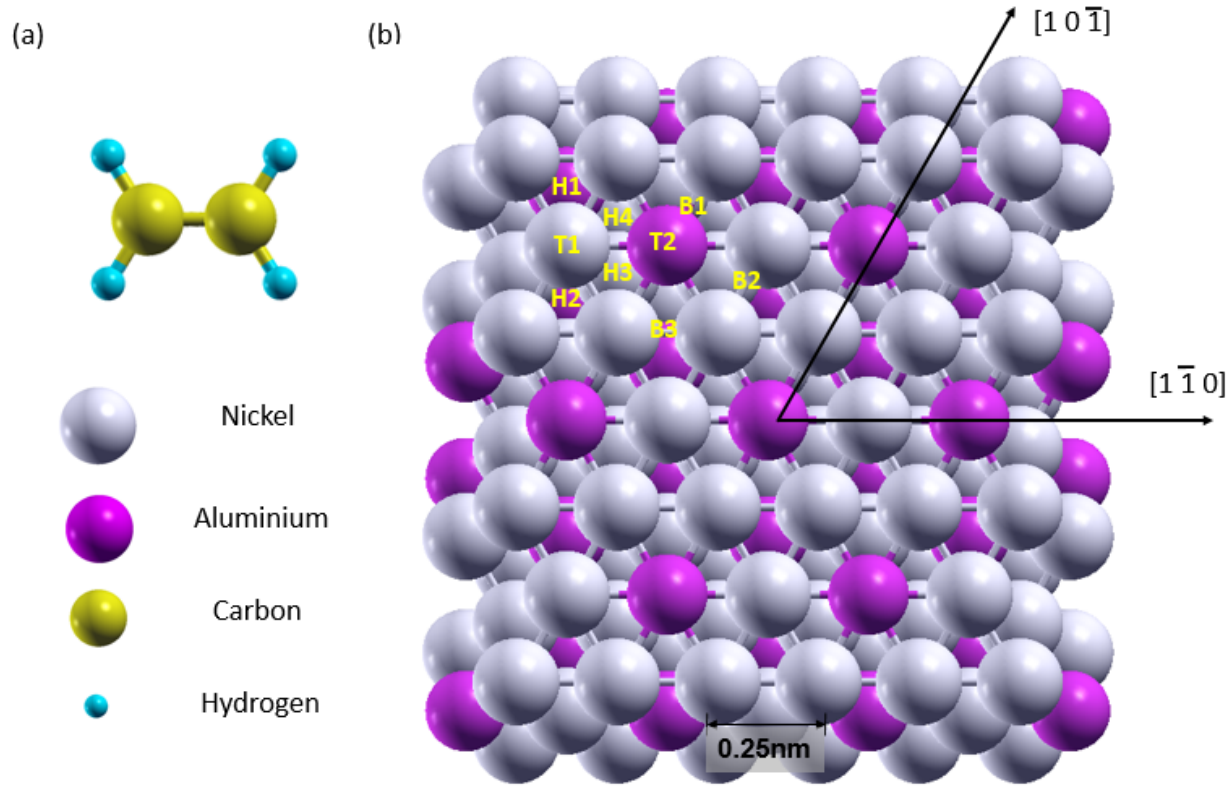

Figure 1. (a) The ethylene molecule and (b) the $Ni_3Al(111)$ substrate. Nine non-equivalent adsorption sites exist on the surface: top Ni (T1), top Al (T2), bridge Ni-Al (B1) and Ni-Ni (B2, B3), hollow between three Ni (H1, H2) and two Ni and one Al atoms (H3, H4).

Adsorption configurations of the hydrocarbon species. A conversion of ethylene into carbon-only species, such as carbon monomers and dimers, can be envisaged as a result of a complex set of chemical reactions which may include, at each elementary step, dehydrogenation, hydrogenation, isomerization, C-C bond cleavage, and the inverse C-C bond formation reactions on the surface. These reactions lead to a family of various C_nH_m (n=1,2 and m=0,1,2,3) products that could appear as intermediate species in the conversion process. Therefore, we start our analysis by identifying the most stable adsorption configurations for all these surface species, including possible energetically degenerate configurations. In Fig. 2 we show fourteen species in their most stable adsorption geometries, together with the corresponding adsorption energies. The species containing only one carbon atom (C, CH, CH_2, CH_3) minimize their energy when the C atom is in a hollow site among three Ni atoms, with an underlying Al immediately below (site H1, see Fig. 1). The same configurations on site H2 (with the underlying Al belonging to the third layer) are typically ~0.25 eV less stable. In some of the species containing two C atoms (C-C, CH-C, CH-CH) each of them adsorbs in different hollow sites, while in others (CH_2-C, CH_2-CH, CH_3-C, CH_3-

CH) only one C atom is bonded to the surface. Ethylene (CH_2-CH_2) has the lowest energy configuration when both C atoms are on the B3 bridge sites of two Ni atoms (structure 11, Fig. 2), but an almost degenerate configuration with a similar adsorption energy has been found (structure 12, Fig. 2). For three species (C-C, CH-C and CH_2-CH_2), we also find several essentially degenerate configurations with adsorption energies differing by no more than 20 meV.

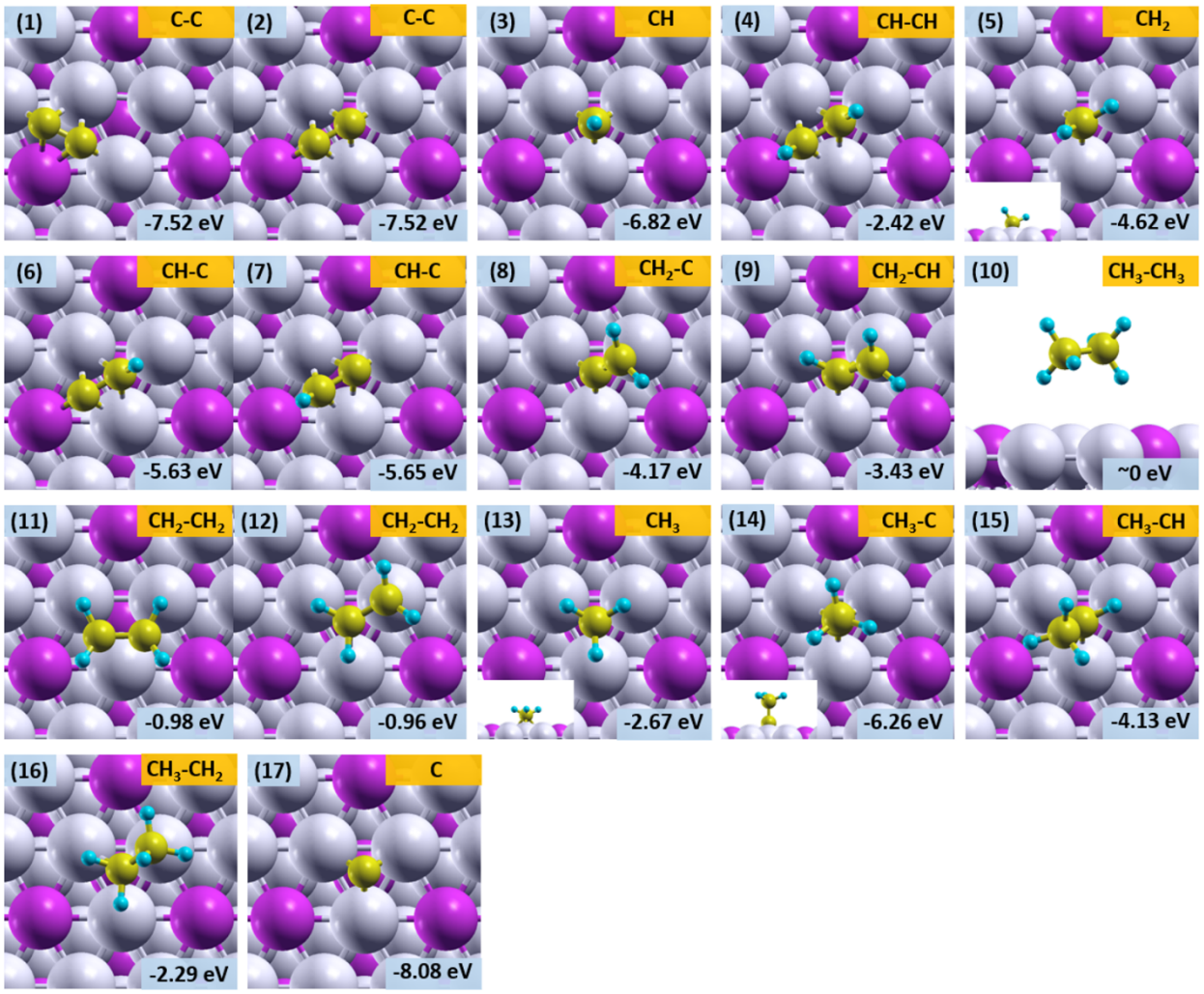

Figure 2. Stable configurations (top views) of the fourteen ethylene derivatives C_nH_m (n=1,2 and m=0,1,2,3), with the corresponding adsorption energies. Adsorbed CH_3-CH_3 (ethane, panel 10) was found to be unstable. As for C-C, CH-C and CH_2-CH_2 species, two degenerate configurations are found (panels 1-2, 6-7, 11-12).

Energy barriers. The optimized molecular geometries in Fig. 2 serve as preliminary information to compute the activation energy barriers associated with every reaction connecting a reactant to all its possible products. In the following, the Nudged Elastic Band (NEB) method[36] is used to calculate the forward and backward barriers corresponding to each

reaction. These data will enable us to identify the most probable reaction paths connecting ethylene to pure carbon species later on. Clearly, more than one path is possible in this "space of products", opening up different scenarios about the temperature evolution of the species on the surface. The stable geometries of the species are used as initial and final states of the reactions, which include the following processes: (*i*) H removal from a species (dehydrogenation); (*ii*) H atom moving from one carbon to the other (isomerization); (*iii*) C-C bond breaking. The barriers for hydrogenation, reverse isomerization, and C-C association reactions are obtained automatically as corresponding reverse reactions. In Table 1 we show a complete set of reactions, each with the calculated forward (E_{for}) and backward (E_{back}) energy barriers.

No.	Reaction	E_{for}	E_{back}
R1	CH_2-CH_2 → CH_2-CH + H	0.75	0.75
R2	CH_3-CH_2 → CH_2-CH_2 + H	0.23	0.68
R3	CH_2-CH → CH_2-C + H	0.38	0.91
R4	CH_3-CH → CH_2-CH + H	0.49	0.67
R5	CH_3-CH_2 → CH_3-CH + H	0.62	0.91
R6	CH_3-CH_3 → CH_3-CH_2 + H	0.90	0.84
R7	CH_3-C → CH_2-C + H	1.01	0.91
R8	CH_3-CH → CH_3-C + H	0.22	1.02
R9	CH_2-CH_2 → CH_3-CH	1.77	1.61
R10	CH_2-CH → CH_3-C	1.45	2.08
R11	CH_2-C → CH-C + H	1.18	1.08
R12	CH-C → C-C +H	1.17	0.86
R13	CH-CH → CH-C + H	1.30	1.05
R14	CH_2-CH → CH-CH + H	0.37	1.08
R15	CH_2-C → CH-CH	2.14	2.30
R16	CH_3 → CH_2 + H	0.87	0.84
R17	CH_2 → CH + H	0.36	0.91
R18	CH → C + H	1.35	1.20
R19	CH_2-CH_2 → CH_2 + CH_2	1.31	0.70
R20	CH_3-CH_2 → CH_3 + CH_2	1.04	0.87
R21	CH_3-CH → CH_3 + CH	0.59	0.71
R22	CH_2-CH → CH_2 + CH	0.79	0.70
R23	CH_2–C → CH_2 + C	1.41	0.64
R24	CH-CH → CH + CH	1.69	1.44

R25	**CH-C → CH + C**	1.76	1.60
R26	**C-C → C + C**	2.12	2.10
R27	**CH_3-C → CH_3 + C**	2.07	1.25
R28	**H diffusion**	0.60	0.60
R29	**H + H → H_2**	1.34	0.05

Table 1. Minimum energy barriers (in eV) associated with reactions involving the ethylene derived reactants shown in Fig. 1. E_{for} and E_{back} indicate, respectively, forward and backward barriers with respect to the direction of the arrow. Dehydrogenation/hydrogenation reactions are indicated in black, isomerization reactions in red and C-C cleavage/bonding in blue. Processes involving H atoms only (R28 and R29) are indicated in magenta. In the final (initial) states of dehydrogenation (hydrogenation) processes, the detached H atom was always relaxed nearby the dehydrogenated species, in an H1 hollow adsorption site, which we found to be the most stable for the H atom placed alone on the surface (see Supporting Information, Sec. SI-1).

The energy barriers are in the range 0.2 eV to 2.5 eV. Isomerization reactions (Table 1, in red) have barriers between 1.45 eV and 2.14 eV, and are higher on average than most of the dehydrogenation barriers (in black), and for this reason are expected to hardly be observed during the decomposition process. In most cases, dehydrogenations barriers tend to be lower than hydrogenation barriers (by comparing E_{for} with E_{back}), the exceptions being reactions R6, R7, R11-R13, and R18. This is an indication, as found experimentally[25], that the formation of graphene on Ni_3Al by ethylene CVD process at high temperature is possible, *i.e.* dehydrogenation reactions may be capable of converting ethylene into carbon-only species. Next, C-C bond breaking barriers (in blue) are between 0.6 and 2.1 eV, and, in most cases, are higher than dehydrogenation barriers (0.22-1.35 eV). However, in order to find probable reaction paths, it is important to include C-C cleavage processes, the most favorable of which can still compete with dehydrogenation processes[18] and play an important role.

The reaction scheme based on the energy barriers in Table 1 is presented in Fig. 3 (*cf.* Refs. 11,12,13,14,15,16,17,18,19,20,21,22,23), and it allows to propose several reactions paths by considering directions with the lowest reaction barriers. Let us consider a TPG experiment when the initially low substrate temperature is gradually ramped up. Initially, when only ethylene is present on the substrate, the lowest reaction barrier corresponds to a hydrogenation process (0.68 eV). However, hydrogenation is (at the very beginning) unavailable for ethylene due to the lack of free H atoms diffusing on the surface. Even allowing for a small initial concentration of them, according to our calculations, the CH_3-CH_2 product would easily revert back to ethylene (E_{back} = 0.23 eV) rather than following

alternative (and more expensive) channels either leading to ethane (CH_3-CH_3, 0.84 eV, which is unstable, as shown in Fig. 2), or to the ethylene isomer CH_3-CH (0.62 eV).

We therefore analyze at first paths that are composed by a sequence of dehydrogenations, making an assumption that no C-C cleavage reaction happen at the early stages. According to the calculated reaction barriers, ethylene should first go towards CH_2-CH (0.75 eV). Then, in the next dehydrogenation process, two products (CH_2-C and CH-CH) are available, with relatively low and very similar energy barriers (0.38 eV and 0.37 eV, respectively). Once CH_2-C and CH-CH are formed, likely in similar quantities, they will be present for some time during the heating, as all other barriers from them are much larger. However, as the temperature is increased, some of the channels become increasingly available. Note also that at this stage free H atoms are also available on the surface: the hydrogenation reaction from CH-CH to CH_2-CH has the lowest barrier available (1.08 eV). Hence, if H atoms are present in the vicinity of CH-CH species, they may convert it to CH_2-CH with subsequent dehydrogenation either back to CH-CH or to CH_2-C. In turn, the latter species may evolve via hydrogenation either to CH_2-CH (0.91 eV), or CH_3-C (also 0.91 eV). If the latter species is formed, it might survive for some time before most probably converting back to CH_2-C, since conversion to CH_3-CH (1.02 eV) has a very low energy barrier (0.22 eV) for the reverse reaction. With further increase of the temperature, CH-CH will be able to dehydrogenate into CH-C (1.30 eV), while breaking the C-C bond has a much higher barrier (1.69 eV). CH_2-C may also dehydrogenate towards the same product CH-C (1.18 eV), which is the species where the two branches (from CH_2-CH to either CH-CH or CH_2-C) reconnect. CH-C could undergo a further dehydrogenation towards C-C (1.17 eV), finally forming a carbon dimer. The C-C cleavage for the dimer is associated with a very high energy barrier (2.12 eV), and so the dimer becomes the final species of this conversion path. In summary, a reasonable scenario based on a sequence of dehydrogenations is given by either of the two paths:

1. CH_2-CH_2 => CH_2-CH + H => CH-CH + 2H => CH-C + 3H => C-C + 4H
   (the highest barrier is 1.30 eV, due to CH-CH => CH-C + H)
2. CH_2-CH_2 => CH_2-CH + H => CH_2-C + 2H => CH-C + 3H => C-C + 4H
   (the highest barrier is 1.18 eV, due to CH_2-C => CH-C + H)

Both these mechanisms result in one carbon dimer (C-C).

Another relevant scenario emerges considering the possibility of C-C cleavage happening already at very early stages. It seems unlikely that this would happen immediately

(ethylene C-C cleavage, 1.31 eV), as the reverse association reaction (0.70 eV) would reform the ethylene molecule. However, the C-C cleavage is much more favorable in the cases of CH_2-CH (0.79 eV) and CH_3-CH (the species with the lowest cost for C-C breaking, 0.59 eV). Hence, two monomer-producing paths emerge. The first one is characterized by the C-C cleavage in CH_2-CH:

3. CH_2-CH_2 => CH_2-CH + H => CH_2 + CH + H => 2CH + 2H => 2C + 4H
   (the highest barrier is 1.35 eV at the final stage due to CH=> C+H)

where the last two steps are dehydrogenation processes of the separate species CH_2 (0.36 eV) and CH (1.35 eV). The second scenario is related to the decomposition of CH_3-CH:

4. CH_2-CH_2 => CH_2-CH+H => CH_3-CH => CH_3+CH
   (the highest barrier is 1.35 eV, due to the final reaction CH=> C+H)

followed by a sequence of dehydrogenations involving CH_3 (0.87eV) and CH. Note that C-C cleavage reaction of CH_3-CH in this latter path will be competing with a more favourable dehydrogenation to CH_3-C (0.22 eV). This latter species will remain stable until the temperature is sufficiently high for CH_3-C to either dehydrogenate to CH_2-C (1.01. eV) or hydrogenate back to CH_3-CH (1.02 eV). Another competing possibility is for the dehydrogenation of CH_3-CH to CH_2-CH (0.49 eV), which is also more favorable than the C-C cleavage of CH_2-CH. The hydrogenation processes involving CH_2-CH and CH_3-C must be feasible at this stage, considering that hydrogens would preferentially diffuse as single atoms on the surface (0.60 eV, process R28 in Table 1) rather than forming H_2 molecules (1.34 eV, R29), which would eventually desorb from the surface.

It is interesting to compare these results, based solely on energy barriers, with the ones obtained on ethylene decomposition on Ir(111)[18]. The most striking difference is that the most probable pathway proposed on Ir(111) involves the C-C cleavage of the CH-CH species (the calculated energy barrier is 0.85 eV). This value is half of our barrier (1.69 eV) on Ni_3Al(111), preventing one to consider this particular cleavage as a part of a probable path on this substrate.

Note that C-C cleavage Ni_3Al(111) is increasingly more difficult for species that are already dehydrogenated. Hence, without considering backwards processes, we expect that the C-C bond scission should happen at the early stages (as in paths 3 and 4); otherwise, the most probable mechanisms must be the sequences proposed in paths 1 and 2. We also note that competition between various processes, including those outlined above, is not only due to similarity of the energy barriers; the actual outcome is also dependent on the spatial

availability of the species and their concentration (or, reversely, on the availability of the empty space for the products). For instance, for hydrogenation reactions it is required that a sufficient amount of H atoms is available on the surface. All these factors would affect the final mechanism (see, *e.g.* Ref. 18), and are hardly predictable considering the reaction barriers alone.

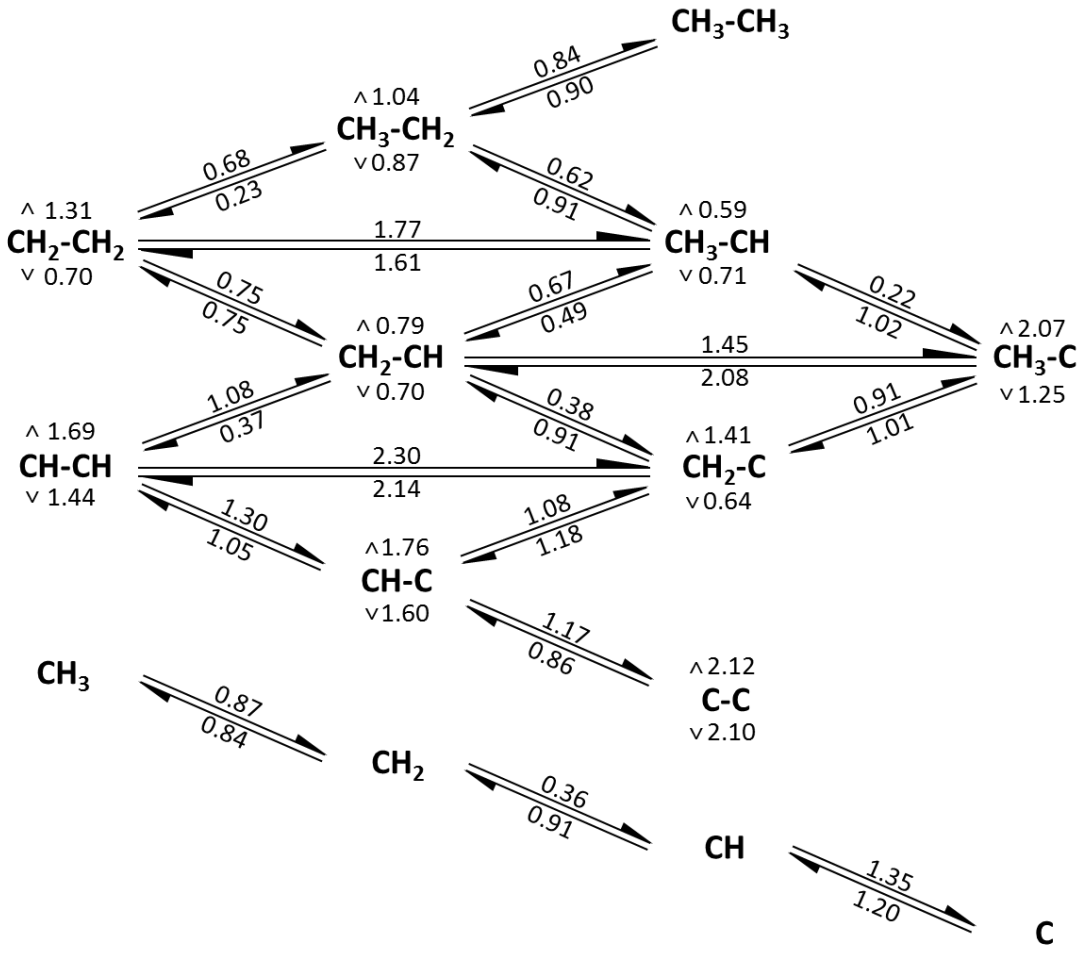

Figure 3. The complete reaction scheme with combined DFT and NEB calculated energy barriers. Barriers above (below) arrows represent forward (backwards) reactions, with values expressed in eV. Barriers above (below) species symbols with marks □ (□) correspond the C-C bonds breaking (forming) processes.

X-ray Photoelectron Spectroscopy measurements and calculated C 1s core level shifts. TP-XPS experiments have been performed by acquiring *in situ* XPS spectra at normal emission, with a photon energy of 400 eV, while annealing the $Ni_3Al(111)$ surface after C_2H_4 exposure at T=80 K until saturation, which corresponds to 0.4 ML of carbon coverage. The

initial C 1s spectrum, corresponding to the saturated ethylene surface (see Fig. 4) can be fitted with two components, shifted by 0.56 eV, whose intensities are in a ratio of 3.2 : 1. The spectrum was fitted with Doniach-Sunjic functions[37], which are characterized by two parameters: the singularity index α describes the asymmetry due to the excitation of electron-hole pairs near the Fermi level, while the Lorentzian width is due to the finite core-hole lifetime. The resulting function has been convoluted with a Gaussian, taking into account the broadening due to vibrational/phonon and inhomogeneous effects and an instrumental resolution. The inelastic contribution to the photoemission spectra was described with a linear background.

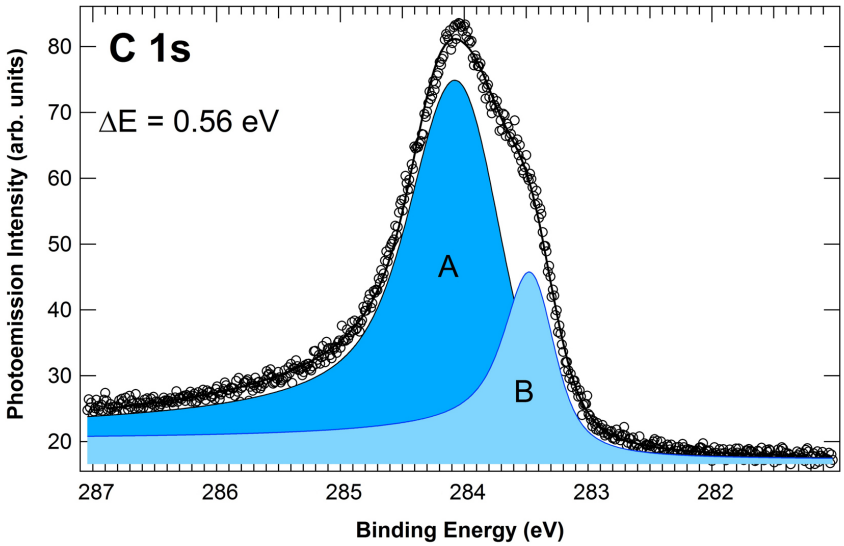

Figure 4: XPS spectrum for the C 1s core level measured on the $Ni_3Al(111)$ surface after ethylene exposure at T=80K until saturation (0.4 ML of carbon coverage). The two observed components have a shift of 0.56 eV and their intensities are in a ratio of 3.2 : 1.

In order to interpret the XPS spectrum at low temperature and to gain information about the ethylene adsorption geometry, we resorted to C 1s DFT calculations. The values of the C 1s core level shifts for the different species and for non-equivalent carbon atoms they contain are shown in Fig. 5. The C 1s binding energy of the carbon atoms in ethylene in its most stable configuration was chosen as the reference core level binding energy (see Fig. 5, panel 1), so that all core level shifts are reported with respect to this value. It is important to underline that the two C_2H_4 species, denoted CH_2-CH_2(a) and CH_2-CH_2(b) in the following (shown in panels 11 and 12 in Figure 2, respectively), are energetically almost degenerate, displaying adsorption energies that differ by only 0.02 eV, and are therefore expected to have

quite similar occupation probabilities when exposing the surface to ethylene at low temperature. Interestingly, while the calculated core level shifts for the two carbon atoms of the species CH_2-CH_2(a) are both zero due to their local environments being identical (as the geometry is symmetric), the other species CH_2-CH_2(b) shows C 1s shifts of +0.09 eV and -0.64 eV for the two non-equivalent carbon atoms. Therefore, the measured C 1s spectrum can be interpreted as due to ethylene molecules adsorbed in different geometries: the E1 component is generated by CH_2-CH_2(a) molecules (Fig. 5, panel 1) and by the carbon atoms of the CH_2-CH_2(b) type molecule at the top site (Fig. 5, panel 2), while the E2 component arises from C atoms of CH_2-CH_2(b)-type molecules placed at the three-fold site (Fig. 5, panel 3). Assuming that the surface occupations of the CH_2-CH_2(a) and CH_2-CH_2(b) species are identical, we would indeed expect the two components of the C 1s spectrum relative intensities to be in the 3:1 ratio, which is very close to the experimental findings, and with a full width of the E1 component larger than for E2, as would be expected.

The C 1s identification of the two non-equivalent ethylene molecules probed at low temperature allowed us to align the calculated C 1s core electron binding energy scale with the experimental one. The saturated layer obtained after exposing the $Ni_3Al(111)$ to C_2H_4 at T=80 K was then annealed with a linear temperature ramp (0.25 K/s) while monitoring in real-time the evolution of the C 1s core level spectrum. The results are shown in Fig. 6 (lower panel) as a two-dimensional plot, where each horizontal line corresponds to a single XPS spectrum. Superimposed on the experimental data are the calculated values of the core level shifts corresponding to all the different species that have been investigated in this work (both panels). Note that the CH-C species adopts two geometries (will be denoted (a) and (b), respectively, as shown in panels 6 and 7 in Fig. 2) which are basically energy degenerate; however, if for species (a) the two C 1s electron binding energies are quite different (panels 6 and 7 in Fig. 5), for the other species (b) they are very close (panels 8 and 9 in Fig. 5). The main spectral C 1s changes can be appreciated (i) at about 160 K with a general shift of the spectral intensity to lower binding energy values, (ii) between 200 K and 350 K when the spectrum displays a general loss of spectral intensity at high binding energy values, while displaying growth of the main component at 283.2 eV, and (ii) above 400 K when the C 1s peak start shifting to higher binding energies. The calculated core level shifts which are within the measured energy range, besides the CH_2–CH_2(a) and CH_2–CH_2(b) species, include those corresponding to CH_2–CH, CH_2–C, and CH–C(b) (lower panel in Fig. 6).

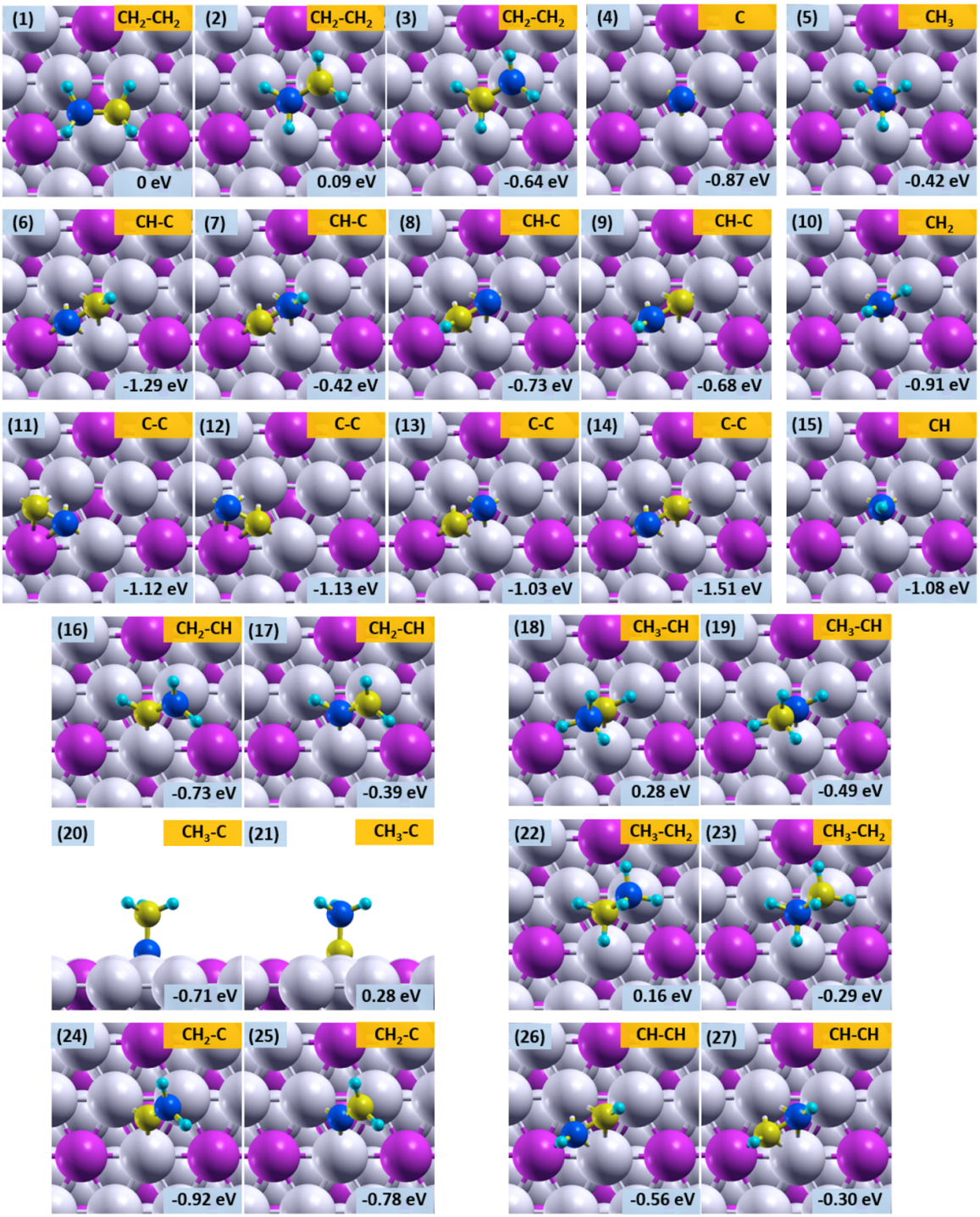

Figure 5. C 1s core level shifts calculated for all non-equivalent carbon atoms within all hydrocarbon species on $Ni_3Al(111)$. All values are referred to one of the two equivalent C atoms of the ethylene molecule on the surface. The blue atom on each panel corresponds to the carbon atom for which the CLS was actually calculated.

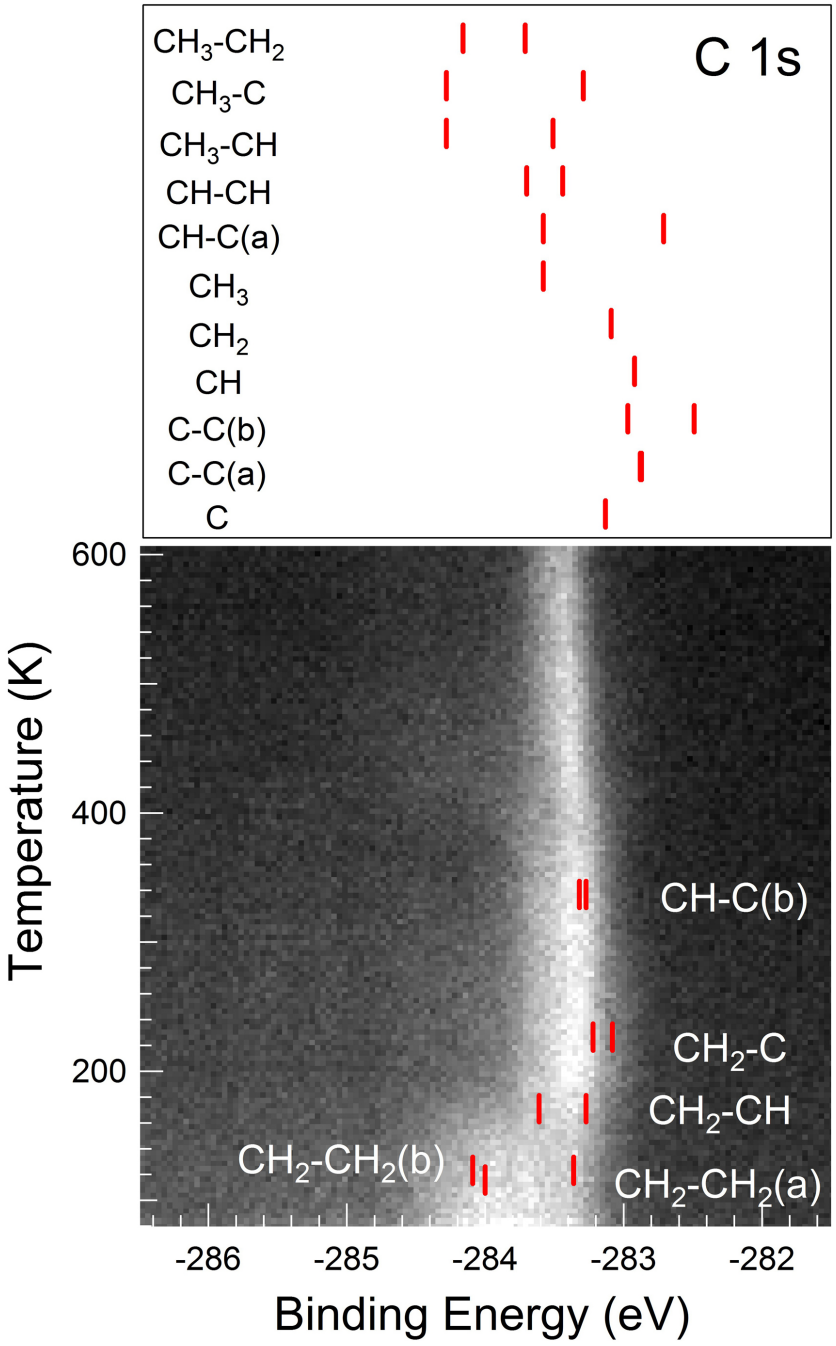

Figure 6: Upper panel: DFT calculated core level shifts for all non-equivalent C atoms of the species indicated. Lower panel: XPS spectra of the surface after ethylene exposure annealed with a linear temperature ramp (0.25 K/s) from T=80 K. The calculated core level shifts for the rest of the species considered in this work are superimposed on the experimental spectra. More than two shifts are given in the cases of structural degeneracies some species have on the Ni_3Al substrate (CH_2-CH_2, CH-C, and C-C).

Combining the TP-XPS spectra and the calculated C 1s core level shifts (Fig. 6), we can see that some species belonging to the proposed dissociation paths display a match between calculated and observed C 1s binding energy values (in the order of increasing temperature):

CH_2-CH_2, CH_2-CH, CH_2-C, and CH-C, all of which belong to path 2. Furthermore, regarding CH-CH, in temperature range (ii) a gain of spectral intensity at high binding energy values would be expected, but is not observed, therefore excluding path 1. It is interesting that acetylene is not detected (unlike in other systems), but this is actually in agreement with our theoretical findings which show that reaction path 1 is not the minimum energy one. However, we cannot exclude that CH-CH diffuses very rapidly away and cyclizes on the surface[38, 39]. For CH_3-CH and for CH, except in temperature range (i) where in any case only ethylene is adsorbed, the spectra are not compatible with the presence of these species on the surface. This allows us to exclude paths 3 and 4. According to these results, until 400 K, the best agreement of the TP-XPS data is with path two (CH_2-CH_2 => CH_2-CH => CH_2-C => CH-C=> C-C), which is the most likely among the four paths suggested above. The other paths, which were considered possible based on the reaction barriers alone, are not experimentally observed, probably as a result of kinetic effects, the investigation of which we leave for a future study.

However, according to the proposed dissociation path, carbon dimers should result from the decomposition process; it is possible that carbon monomers may also be present, albeit in smaller quantities, due to either other decomposition paths or dissociation of the carbon dimers (the barrier for the latter process is however rather large, 2.1 eV, see Fig. 3, so even at elevated temperatures the overall yield of this process is expected to be small). In any case, the spectra in temperature range (iii) do not correspond to either C or C-C, so that carbon monomers and dimers are not detected experimentally. In order to explain the absence of these species, which should be present regardless of which dissociation path has been followed, the diffusion barriers for carbon monomers and dimers have been calculated. Indeed, they were found to be 1.18 eV and 0.73 eV, respectively (see Sec. SI-3). These barriers are sufficiently low, especially in the case of C-C, so that it is reasonable to conclude that these species are quite mobile on the surface at elevated temperatures. Hence, we conclude that the carbon dimers resulting from the proposed dissociation path can diffuse rapidly on the surface and easily combine into larger carbon clusters, giving short lifetimes for these species, and resulting in spectra that lack the C-C dimer fingerprint.

4 Conclusions

In this work, we employed DFT and Nudged Elastic Band methods to study the early stages of graphene formation on a bimetallic alloy substrate; specifically, we have been concerned

with the thermal decomposition of ethylene on $Ni_3Al(111)$. Recent experimental studies[25] have shown that the use of alloys represent a promising route to the direct synthesis, via oxidation of the alloy-graphene interface, of a wide range of metal-insulator-graphene architectures, very relevant in transistor technology. Due to the general variety, availability and a low cost of bimetallic alloys, the theoretical characterization at the atomic level of the reaction mechanisms on these substrates is important for optimization of the production steps towards industrial applications. Via the calculation of the energy barriers between various species resulting from ethylene on $Ni_3Al(111)$ during the decomposition process, we discussed four possible reaction paths which could lead to carbon-only (hydrogen-free) species on the surface necessary for subsequent graphene nucleation and growth: two are based on a sequence of dehydrogenations and result in carbon dimers, and the other two stem from favorable C-C cleavage reactions followed by dehydrogenations and ultimately leading to carbon monomers. Core energy level shifts of the carbon atoms in all species and for all degenerate systems are also calculated and compared with high energy resolution XPS experiments, and were used to exclude paths 1, 3, and 4, because important intermediate species for these paths missing in the observed spectra. On the basis of the theoretical results and experimental XPS spectra we are able to conclude that the prevalent decomposition mechanisms of ethylene on the $Ni_3Al(111)$ surface is:

$$CH_2\text{-}CH_2 \Rightarrow CH_2\text{-}CH \Rightarrow CH_2\text{-}C \Rightarrow CH\text{-}C \Rightarrow C\text{-}C.$$

It follows then that one should expect formation of carbon dimers, not monomers, as the overall product of ethylene decomposition on this substrate. However, already at 400 K, these highly mobile species are likely to be almost completely absent due to formation of larger carbon clusters.

We hope that the theoretical data presented in this work will stimulate further experiments and simulations on a variety of combinations of hydrocarbons and bimetals, with the aim of characterizing the catalytic properties of this class of substrates and optimizing the process of synthesis of nanostructures with technological relevance.

Supporting Information. 1) Hydrogen adsorption sites on Ni_3Al (111). 2) Energy barriers and reaction paths. 3) C and C-C diffusion processes on Ni_3Al (111).

6 Acknowledgments

JL and YW gratefully acknowledge financial support from the National Natural Science Foundation of China under Grant No. 11574238. JL, LK and AF would like to thank Holly Tetlow and Chiara Paris for technical help in some calculations. AF and LK thank the EPSRC grant (EP/J019844/1) for funding. Via our membership of the UK's HPC Materials Chemistry Consortium, which is funded by EPSRC (EP/L000202), this work used the ARCHER UK National Supercomputing Service (http://www.archer.ac.uk). AB acknowledges the financial support of the University of Trieste through the program "Finanziamento di Ateneo per progetti di ricerca scientifica – FRA 2014".

References

[1] Novoselov, K. S.; Fal□ko, V.I.; Colombo, L; Gellert, P. R.; Schwab, M.G.; Kim, K. A roadmap for graphene. *Nature* **2012**, *490*, 192-200.

[2] Batzill, M. The surface science of graphene: metal interfaces, CVD synthesis, nanoribbons, chemical modifications, and defects. *Surf. Sci. Rep.* **2012**, *67*, 83-115.

[3] Wang, X.-R.; Tabakman, S. M.; Scott, M.; Dai, H. J. Atomic layer deposition of metal oxides on pristine and functionalized graphene. *J. Am. Chem. Soc.* **2008**, *130*, 8152-8153.

[4] Gao, L.; Ni, G.X.; Liu, Y; Liu, B; Castro Neto, A.H.; Loh K.P. Face-to-face transfer of wafer-scale graphene films. *Nature* **2014**, *505*, 190-194.

[5] Tetlow, H.; Posthuma de Boer, J.; Ford, I. J.; Vvedensky, D. D.; Coraux, J.; Kantorovich, L. Growth of epitaxial graphene: Theory and Experiment. *Phys. Rep.* **2014**, *542*, 195-295.

[6] Coraux, J.; N'Diaye, A. T.; Engler, M.; Busse, C.; Wall, D.; Buckanie, N.; zu Heringdorf, F.-J. M.; van Gastel, R.; Poelsema, B.; Michely, T. Growth of graphene on Ir (111). *New J. Phys.* **2009**, *11*, 023006.

[7] Loginova, E.; Bartelt, N. C.; Feibelman, P. J.; McCarty, K. F. Evidence for growth by C cluster attachment. *New J. Phys.* **2008**, *10*, 093026.

[8] Wang, B.; Ma, X.; Cao, M.; Schaub, R.; Li, W.-X. Size-selective carbon nanoclusters as precursors to the growth of epitaxial graphene. *Nano Lett*. **2011**, *11*, 424-430.

[9] Gao, J.; Yip, J.; Zhao, J.; Yakobson, B. I.; Ding, F. Graphene nucleation on transition metal surface: Structure transformation and role of the metal step edge. *J. Am. Chem. Soc*. **2011**, *133*, 5009-5015.

[10] Huang, L.; W-Y., X.; Que, Y.-D.; Pan, Y.; Gao, M.; Pan, L.-D.; Guo, H.-M.; Wang, Y.-L.; Du, S.-X.; Gao, H.-J. The influence of annealing temperature on the morphology of graphene islands. *Chin. Phys. B* **2012**, *21*, 088102.

[11] Zhang, W.; Wu, P.; Li, Z.; Yang, J. First-principles thermodynamics of graphene growth on Cu surfaces. *J. Phys. Chem. C* **2011**, *115*, 17782-17787.

[12] Gajewski, G.; Pao. C. W. *Ab initio* calculations of the reaction pathways for methane decomposition over the Cu(111) surface. *J. Chem. Phys*. **2011**, *135*, 064707.

[13] Zhao, Z.-J.; Moskaleva, L. V.; Aleksandrov, H. A.; Basaran, D.; Rosch, N. Ethylidyne Formation from Ethylene over Pt(111): A mechanistic study from first-principle calculations. *J. Phys. Chem. C* **2010**, *114*, 12190-12201.

[14] Aleksandrov, H. A.; Moskaleva, L. V.; Zhao, Z.-J.; Basaran, D.; Chen, Z.-X.; Mei, D.; Rosch, N. Ethylene conversion to ethylidyne on Pd(111) and Pt(111): A first principles-based Kinetic Monte Carlo study. *J. Catal*. **2012**, *285*, 187-195.

[15] Chen, Y.; Vlachos, D. G. Hydrogenation of ethylene and dehydrogenation and hydrogenolysis of ethane on Pt(111) and Pt(211): A density functional theory study. *J. Phys. Chem. C* **2010,** *114*, 4973-4982.

[16] Watwe, R. M.; Cortright, R. D.; Nørskov, J. K. and Dumesic, J. A. Theoretical studies of stability and reactivity of C_2 hydrocarbon species on Pt clusters, Pt(111), and Pt(211). *J. Phys. Chem. B* **2000**, *104*, 2299-2310.

[17] Basaran D.; Aleksandrov, H. A.; Chen, Z.-X.; Zhao, Z.-J.; Rösch, N. Decomposition of ethylene on transition metal surfaces M(111). A comparative DFT study of model reactions for M= Pd, Pt, Rh, Ni, *J. Mol. Catal. A-Chem*. **2011**, *344*, 37-46.

[18] Tetlow, H.; Posthuma de Boer, J.; Ford, I. J.; Vvedensky, D. D.; Curcio, D.; Omiciuolo, L.; Lizzit, S.; Baraldi, A.; Kantorovich, L. Ethylene decomposition on Ir(111): Initial path to graphene formation. *Phys. Chem. Chem. Phys*. **2016***, 18,* 27897-27909.

[19] Murillo, L. E.; Chen, J.G. A comparative study of the adsorption and hydrogenation of acrolein on Pt(111), Ni(111) film and Pt–Ni–Pt(111) bimetallic surfaces. *Surf. Sci.* **2008**, *602*, 919-931.

[20] Murillo, L. E.; Goda, A. M.; Chen, J. G. Selective hydrogenation of the C=O bond in acrolein through the architecture of bimetallic surface structures. *J. Am. Chem. Soc.* **2007**, *129*, 7101-7105.

[21] Murillo, L.E.; Menning, C.A.; Chen, J. G. Trend in the C=C and C=O bond hydrogenation of acrolein on Pt-M (M = Ni, Co, Cu) bimetallic surfaces. *J. Catal.* **2009**, *268,* 335-342.

[22] Khan, N.A.; Zellner, MB; Chen, JG. Cyclohexene as a chemical probe of the low-temperature hydrogenation activity of Pt/Ni(111) bimetallic surfaces. *Surf. Sci.* **2004**, *556*, 87–100.

[23] Goda, A. M.; Barteau, M. A.; Chen, J. G.; Correlating electronic properties of bimetallic surfaces with reaction pathways of C_2 hydrocarbons. *J. Phys. Chem. B* **2006**, *110*, 11823-11831.

[24] Alfè, D.; Pozzo, M.; Miniussi, E.; Günther, S.; Lacovig, P.; Lizzit, S.; Larciprete, R.; Burgos, B. S.; Mentes, T. O.; Locatelli et al. Fine tuning of graphene-metal adhesion by surface alloying. *Sci. Rep.* **2013**, *3*: 2430.

[25] Omiciuolo, L.; Hernández, E. R.; Miniussi, E.; Orlando, F.; Lacovig, P.; Lizzit, S.; Menteş, T.O.; Locatelli, A.; Larciprete, R.; Bianchi et al. Bottom-up approach for the low-cost synthesis of graphene-alumina nanosheet interfaces using bimetallic alloys. *Nat. Commun.* **2014**, *5*: 5062.

[26] Baraldi, A.; Comelli, G.; Lizzit, S.; Cocco, D.; Paolucci, G.; Rosei, R. Temperature programmed X-ray photoelectron spectroscopy: a new technique for the study of surface kinetics *Surf. Sci.* **1996**, *367*, L67-L72.

[27] Bianchi, M; Cassese, D; Cavallin, A; Comin, R; Orlando, F; Postregna, L; Golfetto, E; Lizzit, S; Baraldi, A. Surface core level shifts of clean and oxygen covered Ir(111). *New J. Phys.* **2009**, *11,* 063002.

[28] Giannozzi, P.; Baroni, S.; Bonini, N.; Calandra, M.; Car, R.; Cavazzoni, C.; Ceresoli, D.; Chiarotti, G. L.; Cococcioni, M.; Dabo, I. et al. QUANTUM ESPRESSO: a modular and

open-source software project fo quantum simulations of materials. *J. Phys.: Condens. Matter* **2009**, *21*, 395502; URL http://www.quantum-espresso.org.

[29] Vanderbilt, D. Soft self-consistent pseudopotentials in a generalized eigenvalue formalism. *Phys. Rev. B* **1990**, *41*, 7892-7895.

[30] Perdew, J. P.; Burke, K.; Ernzerhof, M. Generalized gradient approximation made simple. *Phys. Rev. Lett.* **1996**, *77*, 3865–3868.

[31] Vydrov, O. A.; Voorhis, T. V. Nonlocal van der Waals density functional: The simpler the better. *J. Chem. Phys.* **2010**, *133*, 244103.

[32] Sabatini, R; Gorni, T; de Gironcoli, S. Nonlocal van der Waals density functional made simple and efficient. *Phys. Rev. B* **2013**, *87*, 041108(R).

[33] Kantorovich, L. TETR package, URL:www.mth.kcl.ac.uk/~lev/codes/lev00/index.html.

[34] Lukas Köhler; Georg Kresse. Density functional study of CO on Rh(111*). Phys. Rev. B* **2004**, *70*, 165405.

[35] Vesselli, E; Bianchettin, L; Baraldi, A; Sala, A; Comelli, G; Lizzit, S; Petaccia L; de Gironcoli, S. The $Ni_3Al(111)$ surface structure: experiment and theory. *J. Phys.: Condens. Matter* **2008**, *20*, 195223.

[36] Jónsson, H.; Mills, G.; Jacobsen, K. W. Nudged Elastic Band method for finding minimum energy paths of transitions, in *Classical and Quantum Dynamics in Condensed Phase Simulations,* Eds. B. J. Berne, G. Ciccotti and D. F. Coker (World Scientific) **1998**, 385-404.

[37] Doniach, S; Sunjic, M. Many-electron singularity in X-ray photoemission and X-ray line spectra from metals. *J. Phys. C: Solid State Phys.* **1970**, *3*, 285-291.

[38] Baddeley C.J.; Ormerod R.M.; Stephenson A.W.; Lambert R.M. Surface-structure and reactivity in the cyclization of acetylene to benzene with Pd overlayers and Pd/Au surface alloys on Au(111). J. Phys. Chem. **1995**, *99*, 5146-5151.

[39] Pacchioni, G; Lambert, R. M. Cyclization of acetylene over Pd(111): A theoretical study of reaction mechanisms and surface intermediates. *Surf. Sci.* **1994** *304*, 208-222.

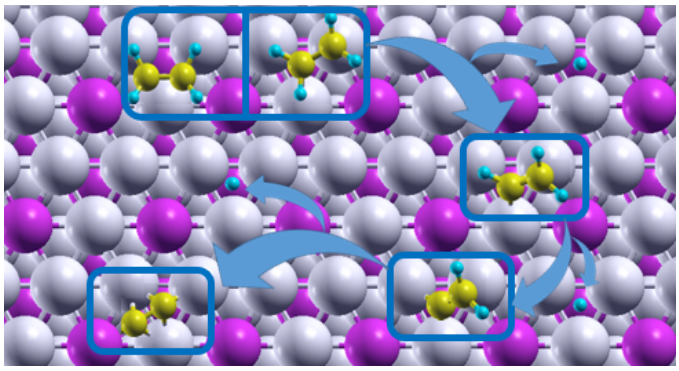

Toc Graphic